Desalination 576 (2024) 117348

Contents lists available at ScienceDirect

Desalination

journal homepage: www.elsevier.com/locate/desal

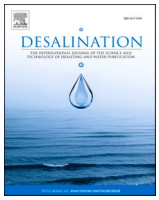

Piloting experience of ROTEC's flow reversal RO (FRRO) for 90 % recovery in brackish water desalination

Mingheng Li [a,*], Alex Waite [b], Sunny Wang [b]

[a] Department of Chemical and Materials Engineering, California State Polytechnic University, 3801 W. Temple Ave., Pomona 91768, CA, United States
[b] City of Santa Monica, 2500 Michigan Ave., Building 1, Santa Monica 90404, CA, United States

HIGHLIGHTS

- Pilot study of flow reversal for ultra-high recovery RO using real water was reported.
- Pilot data were analyzed including specific flux, specific pressure drop and SEC.
- Concentration overshoot during flow reversal was discussed.
- Full-scale retrofit based on pilot study was discussed.

ARTICLE INFO

Keywords:
FRRO
Pilot study
System analysis
Concentration overshoot
Membrane degradation

ABSTRACT

This work reports piloting data analysis of ROTEC's flow reversal RO (FRRO) at City of Santa Monica's Arcadia Water Treatment Plant. It is shown that periodic block rotation and feed flow reversal balance salt and foulant load and mitigate scaling formation, enabling a 90 % recovery with a typical CIP interval over 30 days. As membrane fouls, there is a decline in the specific flux and an increase in the specific pressure drop. Nevertheless, the last stage pressure is usually no more than 200 psi. The successful pilot led to the design and commissioning of the first FRRO full-scale municipal installation in the United States.

1. Introduction

Sustainable and climate resilient water supply is a grand challenge [1]. In seawater reverse osmosis (RO) desalination, pump energy consumption is the single largest factor in the operational expenditures [2,3]. Because pump pressure and specific energy consumption both increase with recovery, the recovery rate in modern seawater RO plants are typically limited in the range of 30–50 %. Brackish water, due to its low salinity, allows a much higher recovery. For example, several brackish RO water plants in Southern California have a recovery of 80–85 %, utilizing 2 to 3 stages [4,5]. Increasing the recovery to 90 % or higher augments water supply and significantly reduces brine management cost, which may be higher than the pump energy cost in inland areas [4]. However, the recovery rate is usually limited by the scaling potential of sparingly soluble minerals (e.g., $CaCO_3$, $CaSO_4$, $BaSO_4$, $SrSO_4$, CaF_2, and SiO_2) in the feed [6–10]. In traditional steady-state design, the tail-end RO elements are exposed to the highest concentration of these scalants indefinitely, unless interrupted by a clean-in-place (CIP) event or permeate flushing. The concentration factor (CF) increases rapidly as the recovery increases above 85 %, and operating at ultra-high recoveries (e.g., 90 % recovery or more) is seldom tried in a full-scale plant. Using antiscalants alone at such a high recovery may not be very effective; they may only slow the precipitation, and overdosing may cause fouling issues [11].

One possible way to mitigate scaling at ultra-high recoveries is transient operation. For example, DuPont/Desalitech's Closed-Circuit RO (CCRO) has been shown to be relatively resistant to fouling [12], because the membrane is periodically flushed by a low-salinity stream. A recent pilot study by Orange County Water District (OCWD) demonstrated the technical feasibility of obtaining a 91 % recovery by using CCRO as the fourth stage to treat brine from its current three-stage RO system [5].

The flow reversal RO (FRRO) developed by Reverse Osmosis Technologies Ltd. (ROTEC) is another example of transient RO. It is based on the conventional three-stage configuration with additional periodic flow reversal and block rotation characteristics. These routinely expose the

* Corresponding author.
E-mail addresses: minghengli@cpp.edu (M. Li), Alex.Waite@santamonica.gov (A. Waite), Sunny.Wang@santamonica.gov (S. Wang).

https://doi.org/10.1016/j.desal.2024.117348
Received 6 October 2023; Received in revised form 9 January 2024; Accepted 15 January 2024
Available online 19 January 2024

most concentrated regions in the RO system to the under-saturated fresh feed, resulting in the dissolution or removal of seed scale particles before they exceed a critical size. Occasionally, feed flow direction to the second stage is also inverted. The FRRO periodically resets the crystallization induction clock and reduces the imbalance of salt/foulant load across all stages. Therefore, it holds the promise of operating at higher recoveries than can be achieved with using anti-scalants alone. Note that ROTEC's concept is slightly different from those in literature [13–17], which focus on feed flow reversal only.

In 2018, the City of Santa Monica embarked on a water supply program to become water self-sufficient by 2023 through the Sustainable Water Master Plan [18]. By maximizing local water resources, the City is able to provide drought-resilient, sustainable, and cost-effective water to its residents in lieu of imported water supplies impacted by climate variability. The program includes additional water conservation, remediation of industrially contaminated groundwater sources, and maximizing alternative water supply opportunities. One alternative supply involves squeezing as much water as possible from the City's existing Arcadia Water Treatment Plant (WTP) groundwater desalting RO process. Preceded by greensand media filtration and cartridge filtration pretreatment, the Arcadia WTP's RO system comprised of four RO trains currently operates at approximately 82–83 % recovery using a conventional three-stage design at a maximum feed flow and flux of 1900 gal per minute (GPM) and 13.5 gal per square foot per day (gfd). The Arcadia WTP provides approximately 60 % of the City's water demand. By increasing recovery to 90 % or greater, the City would be able

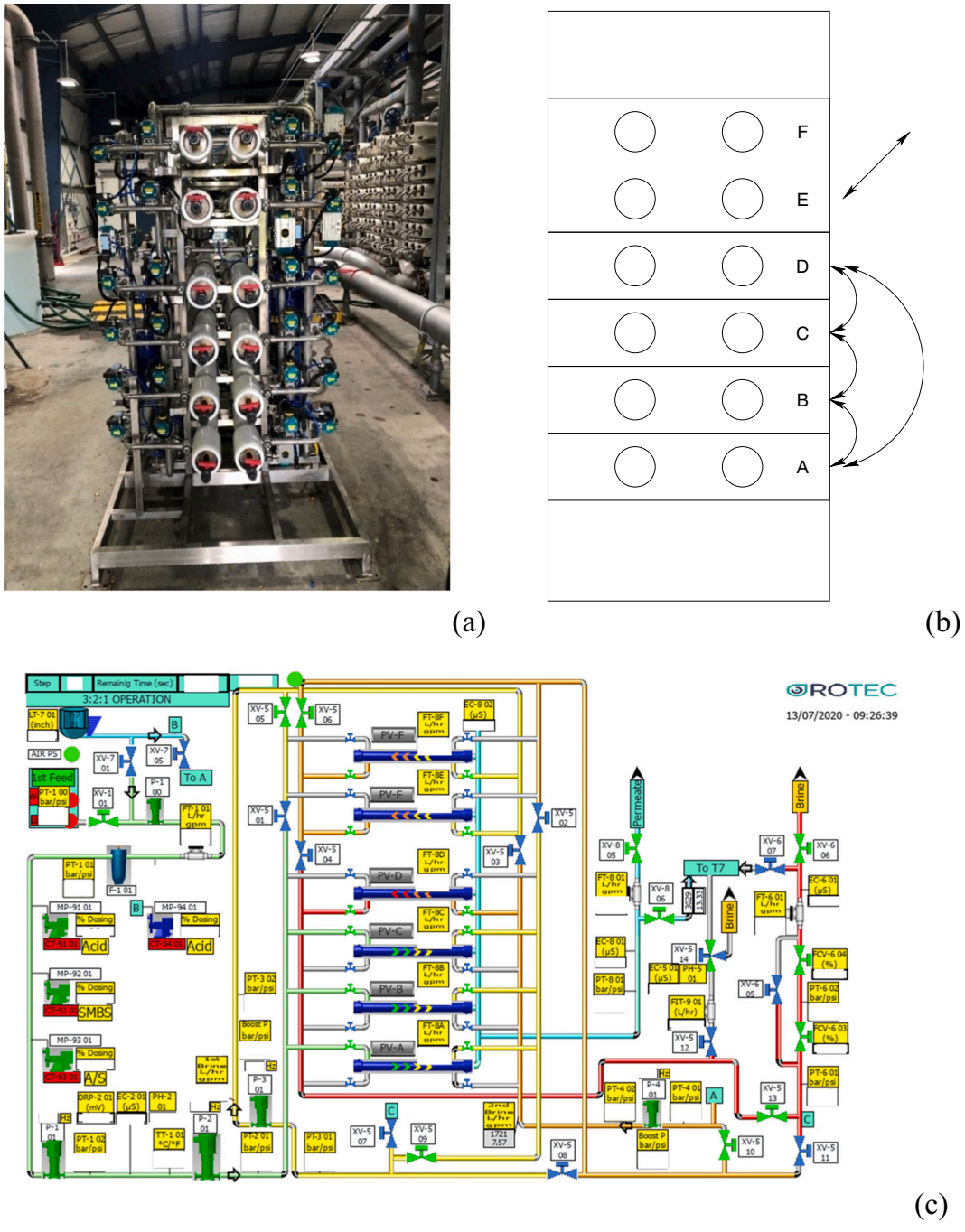

Fig. 1. (a) ROTEC's FRRO pilot skid at City of Santa Monica's Arcadia WTP. (b) Rotation of blocks A-D and feed flow reversal in blocks E and F. (c) Process flow diagram of the pilot system.

to produce an additional 1200 acre-feet per year (AFY) or approximately 10 % of the City's domestic water demand without increasing groundwater production.

A pilot test of ROTEC's FRRO was conducted in 2020 to explore the feasibility of upgrading its current three-stage design using this technology. The pilot testing served to confirm RO permeate water quality (Primarily, TDS $<$ 120 mg/L. More details are provided in supplementary material), to evaluate concentrate stability, and to refine design criteria for the full-scale system that is to be commissioned by 2023. This work presents the pilot results and data analyses. Particularly, a model-based parameter estimation is proposed to track membrane flow and mass transfer characteristics in real time, which may help operation and optimization of the full-scale system.

2. Design and operation of the FRRO pilot

The pilot system is shown in Fig. 1. It consists of 12 pressure vessels, each enclosing three 4" $\times$ 40" Toray TML10D RO elements connected in series. Every two vessels are connected in series to mimic one pressure vessel (or one block) housing six RO elements that is commonly seen in a full-scale system. There are six blocks (A-F) in total. These blocks are arranged in a 3:2:1 array. When the system runs at its full capacity, three out of the four blocks (A, B, C, and D) form the first stage while the remaining block serves as the third stage. Blocks E and F constitute the second stage. The feed flow direction is always forward (i.e. from left to right) in the first stage and reverse (i.e. from right to left) in the third stage. In other words, every time when a block from A-D rotates out to become the third stage, its feed flow direction is reversed. When the third-stage block re-joins the first stage, its feed flow direction returns to forward again. This allows the under-saturated fresh feed to periodically flush the rear-end elements in the previous step. Additionally, the feed flow direction to the second stage switches between forward and reverse at regular intervals. Details about implementing different operation modes via valve switching is provided in the supplementary material. Each system configuration has a designated state number, as shown in Table 1. States 11–14 are similar to 1–4 except that the feed flow direction to the second stage is opposite. State 20 means that the blocks to change state are isolated and disabled temporarily and the system runs at a reduced capacity on remaining blocks before returning to full production.

One full cycle in the pilot test consists of 12 steps, lasting about 450 min (or 7.5 h). The state in each step, its duration time and the transition time between two consecutive steps are shown in Table 2. The production and transition steps in one full cycle are shown in Fig. 2.

The characteristics of the feed water to the RO pilot are shown in Table 3.

The feed is sent to the pilot skid after pretreatment. The pretreatment includes passing through a 5 μm cartridge filter to remove suspend solids, acid dosing to lower the pH of the feed to 6.3, ammonium sulfate dosing to create a 0.5–1.0 ppm monochloramines to inhibit biofouling, and antiscalant dosing of 1 ppm of AWC A-119 (from 6/2 to 9/13/2020) or 2.5–3.0 ppm of Avista Vitec-4000 (from 9/14 to 12/4/2020) recommended by the manufacturers. At 90 % recovery, the scale-forming compounds determined by AWC's Proton Membrane Aqueous Chemistry Calculator [19] include $CaCO_3$ (saturation index = 1.42), $MgCO_3$ (saturation index = 1.03), $CaSO_4$ (saturation index = 0.46), $BaSO_4$ (saturation index = 2.30), CaF_2 (saturation index = 0.21), $CaSi_2O_4$

Table 1
Configuration of blocks in each state.

State	Stage 1	Stage 2	Stage 3
1	BCD	EF (forward)	A
2	CDA	EF (forward)	B
3	BDA	EF (forward)	C
4	ABC	EF (forward)	D
11	BCD	EF (reverse)	A
12	CDA	EF (reverse)	B
13	BDA	EF (reverse)	C
14	ABC	EF (reverse)	D
20	blocks to change state are isolated and repositioned		

Table 2
Operation sequence in one full cycle.

Step	State	Duration (min)	Transition time (min)
1	1	47	5
2	2	47	5
3	3	3	5
4	14	47	5
5	11	47	5
6	12	3	5
7	3	47	5
8	4	47	5
9	1	3	5
10	12	47	5
11	13	47	5
12	14	3	5

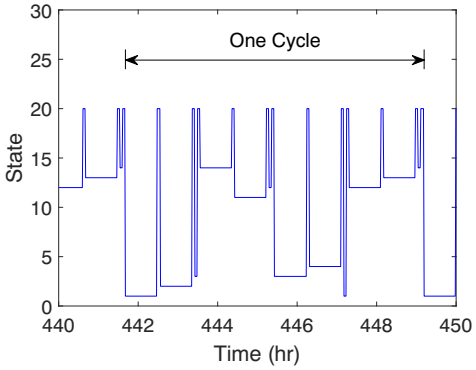

Fig. 2. State of operation in ROTEC's FRRO. $t = 0$ corresponds to 12 am on 9/14/2020.

Table 3
RO pilot feedwater quality prior to pH adjustment and antiscalant addition.

Parameter	Average	Range
Turbidity (NTU)	0.1	0.07–0.12
pH	7.4	7.2–7.7
Conductivity (μS/cm)	1493	1474–1520
Temperature (°F)	71.1	70.0–72.1
Total Chlorine Residual (mg/L)	0.14	0.13–0.15
Dissolved Oxygen (mg/L)	8.4	4.8–11.1
Total Organic Carbon (mg/L)	0.59	0.48–0.72
Total Dissolved Solids (mg/L)	1001	990–1020
Alkalinity (mg/L)	335	330–340
Calcium (mg/L)	144	140–150
Magnesium (mg/L)	61	60–61
Sodium (mg/L)	94	93–96
Potassium (mg/L)	3.2	3.1–3.3
Barium (μg/L)	56	53–61
Chloride (mg/L)	130	120–140
Sulfate (mg/L)	305	300–320
Fluoride (mg/L)	0.31	0.3–0.32
Phosphate (mg/L)	0.06	0.06–0.07
Strontium (mg/L)	0.79	0.78–0.8
Aluminum (total) (μg/L)	10.6	1.3–20.0
Iron (total) (mg/L)	0.03	ND–0.05
Manganese (mg/L)	0.02	ND–0.05
Bromide (μg/L)	523	340–620
Silica (soluble) (mg/L)	37	36–39
Silica (reactive) (mg/L)	38	34–42
Arsenic (μg/L)	1.5	1.2–2.5
Boron (mg/L)	0.19	0.18–0.20
Lead (μg/L)	0.5	0.38–0.59

$(OH)_2$ (saturation index = 3.02), $Mg_3Si_2O_5(OH)_4$ (saturation index = 0.73), and SiO_2 (saturation index = 0.74). The membrane antiscalant software calculation shows that 1.275 ppm AWC A-119 antiscalant dosing delays the formation of inorganic scale for at least two hours [20], which is longer than the cycle time. Silica, calcium silicate and the antiscalant itself are the most likely scaling components, as shown in Fig. 3.

There are two pumps (P1: booster pump and P2: high-pressure pump) before the first stage and two interstage booster pumps (P3 between stages 1 and 2 and P4 between stages 2 and 3). In addition to various valves to direct flow, there are two brine valves (FCV3 and FCV4) to help control the system recovery. The pilot system is equipped with temperature, flow, pressure and conductivity sensors to measure key process variables at various locations. Data are logged every 1 min.

In ROTEC's pilot system, there are 4 controlled variables (feed rate plus either recovery or flux or permeate rate in each stage). There are 6 manipulated variables (speeds of four pumps and positions of two concentrate valves). However, only 4 of them (pumps P2–4 and brine valve FCV4) play the primary role and pump P1 and brine valve FCV3 are auxiliary. The frequency of pump P1 is set to be 22 Hz in state 20 (i.e. during state transition) and 31 Hz in other states (i.e. during normal production). The position of brine valve FCV3 is set to be 61 % in state 20 and 35 % in all other states. Therefore, 4 manipulated variables are able to regulate 4 controlled variables with a zero degree of freedom during normal production. During state transitions, pumps P3 and P4 are turned off temporarily, and 2 manipulated variables (speed of P2 and position of valve FCV4) regulate 2 controlled variables (feed rate plus recovery).

Data from a period of 10 h operation (a little longer than one full cycle) are shown in Figs. 4–7. When the pilot system runs at its full capacity, the flow rate of fresh feed is 30 gpm. At a 90 % recovery during plug-flow operations, each block produces approximately 4.5 gpm of permeate, corresponding to a recovery of 45 %, 55 % and 60 % in the first, second, and third stage, respectively. The average flux on the system level is 14.8 gfd. During a state transition, for example, 1→2, pumps P3 and P4 are turned off for approximately 2 min (Fig. 6) and the RO system has two stages without an interstage booster pump (i.e. blocks CD in stage 1 and blocks EF in stage 2). Feed pumps (P1 and P2) and booster pump before stage 2 (P3) are slowed down to reduce the intake rate (to about 20 gpm) and the system recovery (to about 70 %). At the same time, the positions of both brine valves are increased to accommodate a smaller pressure differential in the feed channels. Pneumatic valves are then actuated so that the block in the third stage (i.e. block A) becomes part of the first stage and the new third stage block (i.e. block B) is engaged. Pump speeds are ramped up and brine valves are closed partially so that flow and recovery return to their normal levels. During certain state transitions (for example, 3→14, 12→3, 1→12, and 14→1), feed flow reversal in blocks *E*-F and rotation in blocks A-D occur at the same time. In such a case, the system is temporarily on one stage with only two blocks (e.g. blocks AB are online during 3→14) and has a recovery about 50 %. The actual system recovery, calculated based on averaged feed and brine flows over a period of 7.5 h (i.e. one full cycle), is 88.2 %.

The feed pressure and pressure differential in each stage, and permeate pressure are shown in Fig. 5. Despite some variations from state to state (due to performance variability in each block that will be discussed later), the system is well behaved. The feed pressure is 137–144 psi in the first stage and 141–146 psi in the second stage. The last stage pressure has a larger temporal variation than the other stages, as the control system responds to a concentration wave travelling throughout all three stages. However, it is no more than 200 psi for an overall recovery of 90 %. The permeate pressure is 7.2 psi during normal production. During state transitions, the permeate pressure reduces to 1 psi because of a sudden reduction in permeate flow.

An instantaneous pressure peak is observed every time the third stage is isolated. As the valves on both ends of the third stage are shut off, the kinetic energy of the moving fluid in the feed channel is transformed into pressure energy. The extent of such a water hammer effect is directly related to the fluid velocity, vessel length and valve closure time. Because the cross velocity is low (0.1–0.2 m/s) and valve closure does not occur instantaneously (approximately 8–10 s closure time), the pressure spikes are not sufficient to cause noticeable damage to the membranes during the pilot test.

Conductivity of fresh feed, permeate and brine are measured in real time. The osmotic pressure in each stream is calculated based on conductivity and temperature and is presented in Fig. 7. The feed conductivity is roughly constant (1565–1585 μS/cm). However, the brine conductivity or concentration varies with block configuration. When the third stage is isolated and disabled, the brine concentration is lower than normal due to a reduced system recovery. When flow reversal in blocks E-F and rotation in blocks A-D occur at the same time, there is always a significant (about 20 %) overshoot in the brine concentration. However,

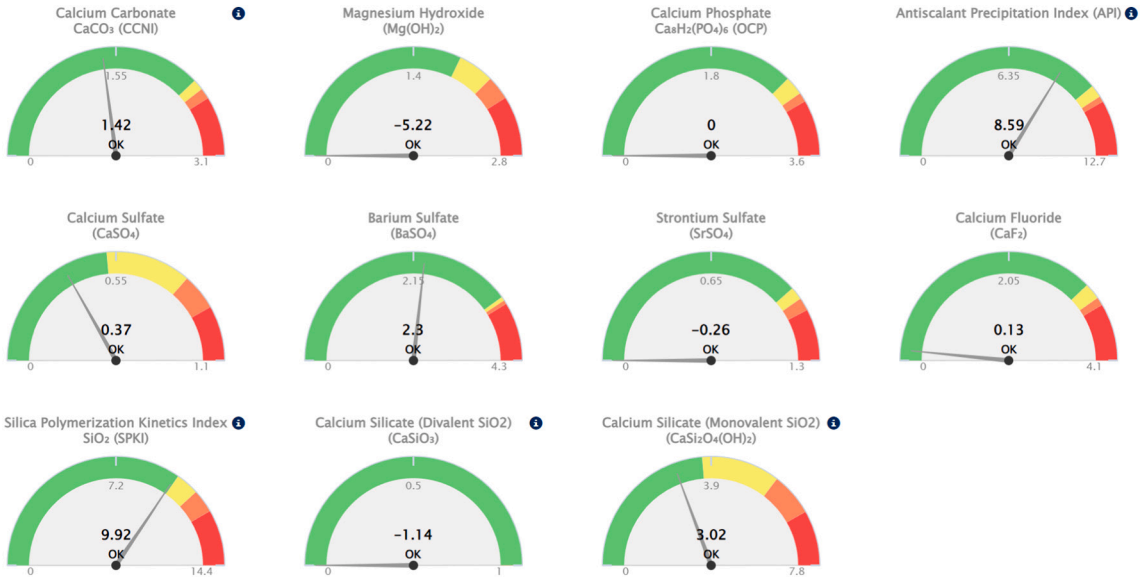

Fig. 3. Scaling predictions based on 1.275 ppm AWC A-119 antiscalant dosing using AWC Proton software (Green: minimum 2 h to failure; Yellow: minimum <2 h-1 h to failure; Orange: <1 h to failure; Red: Instant failure).

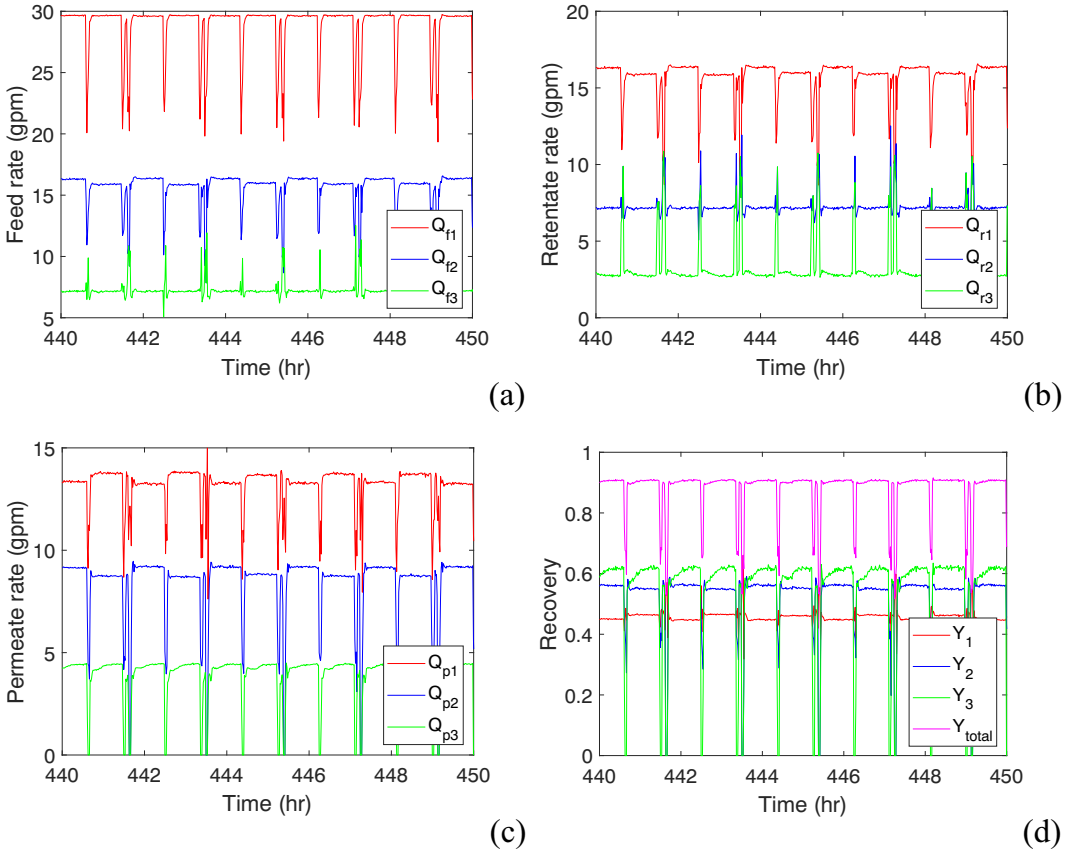

Fig. 4. (a) Feed rate, (b) retentate rate, (c) permeate rate, and (d) recovery in each stage during 10 h of operation.

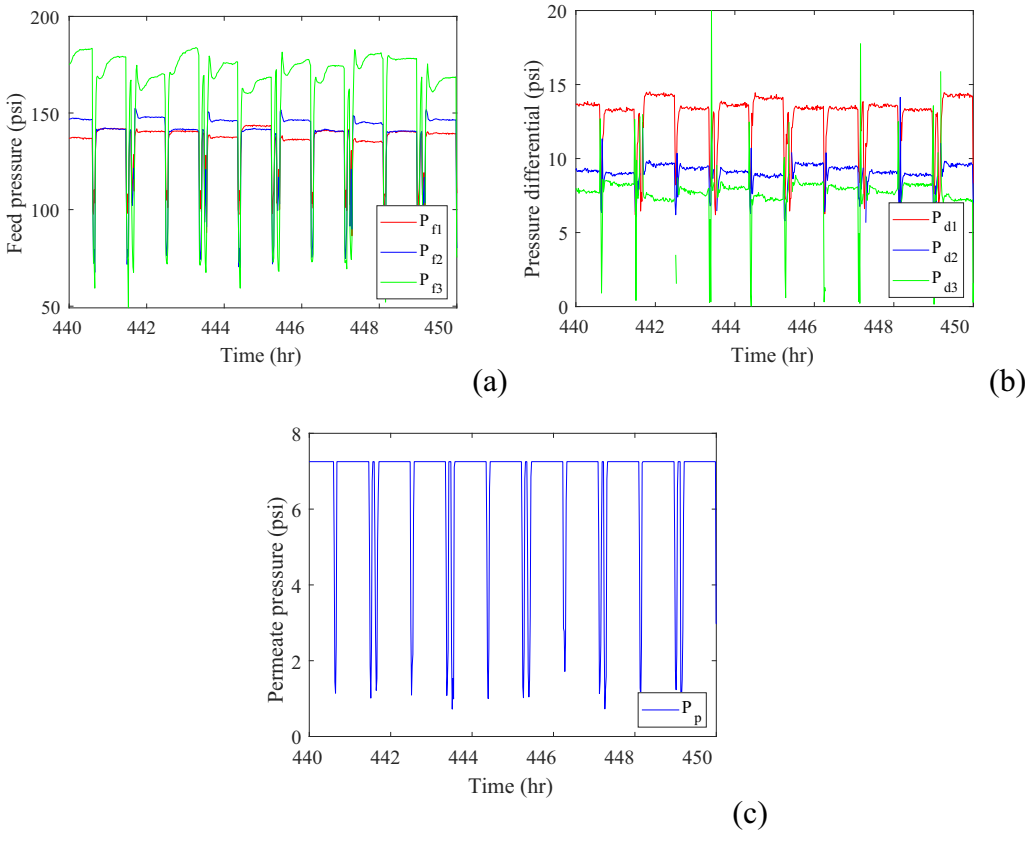

Fig. 5. (a) Feed pressure in each stage, (b) pressure differential in each stage, and (c) permeate pressure during 10 h of operation.

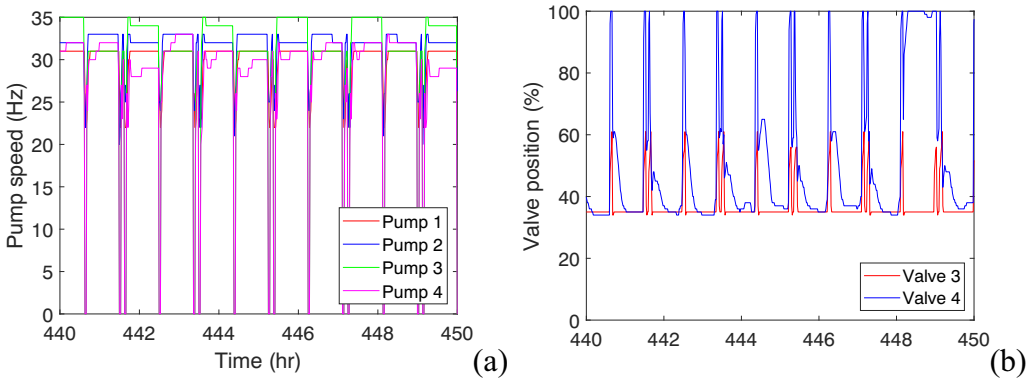

Fig. 6. (a) Speed of pumps and (b) position of brine valves during 10 h of operation.

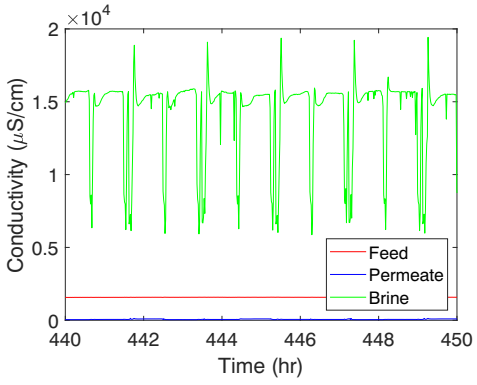

Fig. 7. Conductivities of feed, permeate and brine during 10 h of operation.

when blocks A-D are rotated without reverting the feed flow direction in blocks E-F simultaneously, no large overshoot in the brine concentration is observed. The probable causes will be explained later.

3. Analysis of pilot data

3.1. Mathematical model

Under the assumptions and simplifications of (1) 100 % salt rejection, (2) negligible concentration polarization, and (3) Darcy's law for flux, the following coupled differential equation model was proposed for one RO stage in low-salinity brackish water desalination [21]:

$$-\frac{dQ(x)}{dx} = A_m L_p \left(\Delta P - \frac{Q_f}{Q}\pi_f\right)$$
$$-\frac{d(\Delta P(x))}{dx} = k_f (Q/N_{PV})^n \quad (1)$$

where Q is the flow rate in the pressure vessel, N_{PV} is the total number of pressure vessels connected in parallel (N_{PV} = 3, 2, and 1 for the first, second, and third stage), ΔP is the transmembrane pressure (the difference between retentate pressure P_r and permeate pressure P_p), π_f is the feed osmotic pressure, A_m is the total membrane area in the stage, L_p is the membrane hydraulic permeability. x is dimensionless number with 0, 1, 2, 3 representing inlet of the first stage, outlet of the first stage, outlet of the second stage, and outlet of the third stage respectively. k_f and n are parameters describing the friction loss in the retentate channel. As shown in Fig. 8, $n = 1.5$ can correlate most of the pilot data with an error margin of 10 %. In Fig. 8(a), the arithmetic average of flow rates in the feed channel is used for the correlation. In Fig. 8(b), a linear reduction of feed flow along the stage is assumed. If L_p and k_f are known, Eq. (1) can be integrated to predict pressure and flow at the outlet of each stage. Previous studies of an industrial RO plant showed that such a two-parameter model is capable of predicting system performance of a municipal RO plant [4] and an inclusion of concentration polarization in the model only slightly improves accuracy [22].

Estimation of membrane hydraulic permeability and friction loss parameters from flow and pressure measurements at inlets and outlets of each stage in the pilot test is an inverse problem. Previous plant data show that these parameters may vary over time to time [23]. To estimate them in real time, one may solve a nonlinear regression problem to minimize the difference between plant measurements and predictions

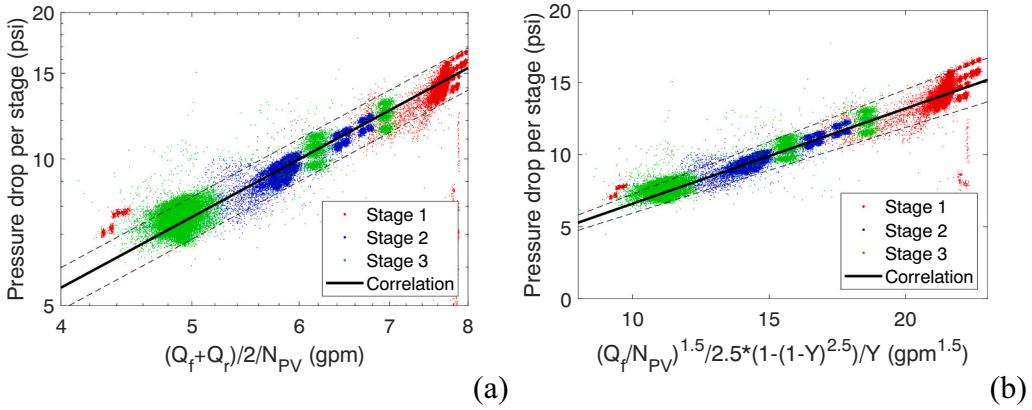

Fig. 8. Retentate pressure drop vs flow rate based on about 30,000 sets of operating data. (a) $P_d = 0.68\left(\frac{Q_f+Q_r}{2N_{PV}}\right)^{1.5}$, (b) $P_d = 0.66\frac{(Q_f/N_{PV})^{1.5}}{2.5}\left[\frac{1-(1-Y)^{2.5}}{Y}\right]$. Dashed lines show ±10% variations.

from Eq. (1) at inlets and outlets of each stage [21]. Fig. 9 is one such example. A particular time ($t = 448.8$ h) is chosen when the membrane is relatively clean (a few days after a CIP event) and the operation is stable. It shows that $L_p = 0.134$ gfd/psi and $k_f = 0.795$ psi/gpm$^{1.5}$ for all stages best fit plant data (difference between model predictions and plant measurements of flow and pressure at every location is less than 3 %). However, if L_p and k_f are allowed to vary slightly ($L_p = 0.132$, 0.137, and 0.135 gfd/psi, $k_f = 0.640$, 0.660, and 0.788 psi/gpm$^{1.5}$ in each stage), a perfect match between model and measurement can be obtained. Stage 3 has a higher apparent pressure drop coefficient probably because the sensors are far away from the inlet and outlet. Fig. 8 does indicate that there are more outliers of the pressure drop data in stage 3.

For real-time monitoring of RO performance, solving such an optimization problem for every time step would be computationally intensive. However, if the driving force and local flux in each stage are assumed to be roughly constant (which is reasonable especially for stages 1 and 2 as suggested by Fig. 9), pressure and flow are decoupled, which makes the calculation much easier.

Based on the simplification of constant flux in a stage, its stage-average osmotic pressure may be calculated by:

$$\begin{aligned}\pi_{r,ave} &= \frac{1}{L}\int_0^L \pi dL \\ &= \frac{1}{Y}\int_0^Y \frac{\pi_f}{1-y}dy \\ &= -\frac{ln(1-Y)}{Y}\pi_f\end{aligned} \tag{2}$$

Note that the brine pressure in one stage is the feed osmotic pressure in the next stage, the average osmotic pressure in each stage are:

$$\begin{aligned}\pi_{1,ave} &= -\frac{ln(1-Y_1)}{Y_1}\pi_0 \\ \pi_{2,ave} &= -\frac{ln(1-Y_2)}{Y_2}\frac{\pi_0}{1-Y_1} \\ \pi_{3,ave} &= -\frac{ln(1-Y_3)}{Y_3}\frac{\pi_0}{(1-Y_1)(1-Y_2)}\end{aligned} \tag{3}$$

where π_0 is the osmotic pressure of the fresh feed, and Y_1, Y_2, and Y_3 are recoveries for stages 1, 2 and 3, respectively.

Under the same simplification, the pressure differential in the retentate channel P_d and the average retentate pressure $P_{r,ave}$ can be approximated by [24]:

$$P_d = \frac{k_f\left(Q_f/N_{PV}\right)^n}{n+1}\frac{1-(1-Y)^{n+1}}{Y} \tag{4}$$

which is used in Fig. 8(b), and

$$P_{r,ave} = P_f - \frac{1+\left[(1-Y)^{n+2}-1\right]/(n+2)/Y}{1-(1-Y)^{n+1}}P_d \tag{5}$$

For $n = 1.5$ and $Y = 0.5$,

$$P_{r,ave} = P_f - 0.58P_d \tag{6}$$

which differs slightly from the equation recommended by membrane manufacturers that assumes linear pressure drop [25]:

$$P_{r,ave} = P_f - 0.5P_d \tag{7}$$

The net driving pressure (NDP) is calculated by:

$$NDP = \left(P_{r,ave} - \pi_{r,ave}\right) - \left(P_p - \pi_p\right) \tag{8}$$

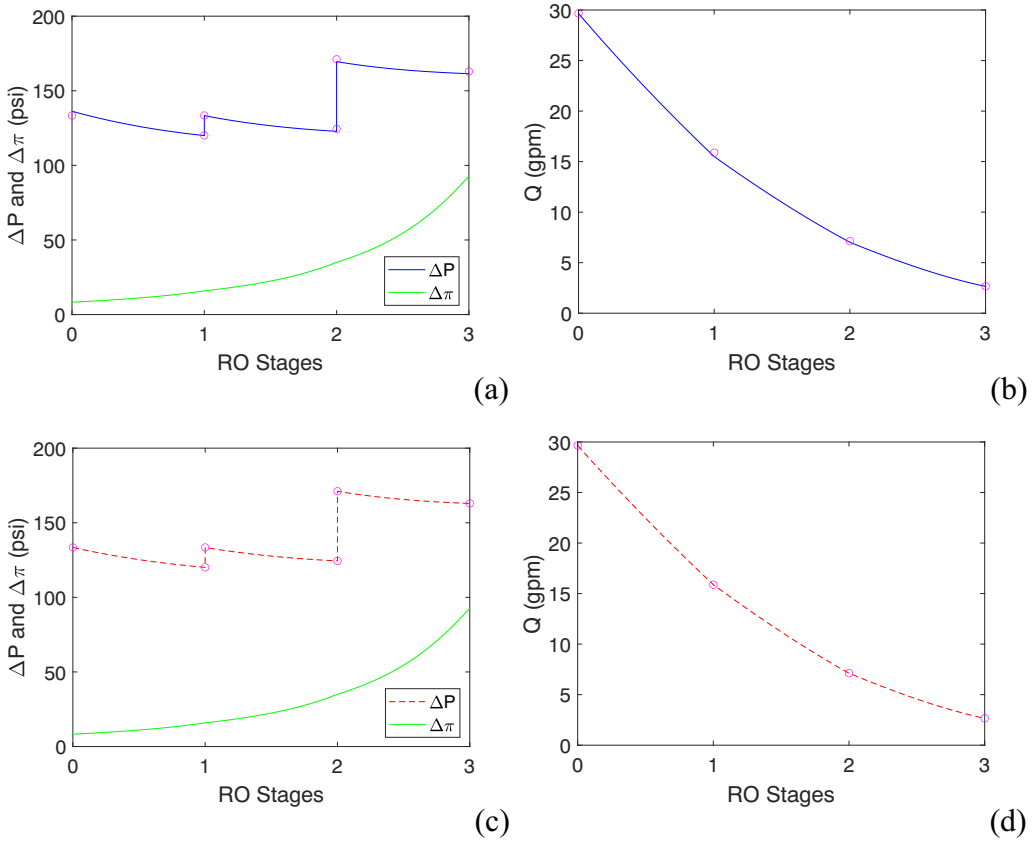

Fig. 9. Comparison of (a), (c) transmembrane pressure and (b), (d) retentate flow rate predicted by mathematical model and plant measurement (circle symbols) when operation is at steady state ($t = 448.8$ h). (a) and (b) are based on the same L_p and k_f in all stages. (c) and (d) are based on stage-specific L_p and k_f.

Under typical operating conditions, π_p is small enough to be safely removed from the above equation.

The average flux of a RO stage $\overline{J}_w$ is calculated by:

$$\overline{J}_w = \frac{Q_f - Q_r}{A_m} \tag{9}$$

where A_m is the total membrane area in the stage.

The membrane hydraulic permeability (or specific flux), L_p, is then calculated by:

$$L_p = \frac{NDP}{\overline{J}_w} \tag{10}$$

The specific pressure drop parameter, k_f, is estimated from Q_f and Y by:

$$k_f = \frac{P_d}{\frac{\left(Q_f / N_{PV}\right)^n}{n+1} \frac{1-(1-Y)^{n+1}}{Y}} \tag{11}$$

A comparison of both parameter estimation methods (nonlinear regression and calculation using Eqs. (10) and (11) assuming approximately constant flux in each stage) is shown in Table 4. The latter method has an error no more than 2 % for stages 1 and 2. The error is larger in stage 3 because the spatial variation in NDP is more significant. For this reason, k_f derived in the third stage should be used for qualitative analysis only.

Note that the method presented above is based on the assumption of steady state operation. To capture dynamics during state transitions, spatiotemporal models are required [26]. As a rule of thumb, it takes several space times to reach steady state.

3.2. Variation in block performance

The average osmotic pressure, NDP, average flux, specific flux, and specific pressure drop in each stage during 10 h of operation are shown in Fig. 10. Spikes shown in Fig. 10(d) and (f) are associated with state transitions and should be ignored. From the regions that are relatively flat, it is seen that the specific flux in the third stage is the lowest when the state is either 2 or 12, implying that block B has the lowest hydraulic permeability among blocks A-D. This is also confirmed by the fact that the highest specific flux in the first stage occurs at state 2 or 12, when block B is rotated out. The opposite trend is consistently found in block A, implying that it has the highest hydraulic permeability among blocks A-D. The feed flow direction in the second stage barely affects the specific flux of each block.

The permeate conductivity is strongly related to the operation state. It is found that the highest permeate conductivity is associated with state 1 or 11 while the lowest is with state 2 or 12. Since stage 3 has the highest salt load, it should contribute the most to the salt passage [27]. This leads to the conclusion that block A has the highest salt permeability while block B has the lowest. The same trend in water and salt permeabilities suggest that the average membrane pore size in block A may be relatively smaller than that in block B.

Table 4
A comparison of two parameter estimation methods.

Parameter	Nonlinear regression	Constant flux approximation	Difference
L_p (gfd/psi), stage 1	0.132	0.132	0 %
L_p (gfd/psi), stage 2	0.137	0.136	0 %
L_p (gfd/psi), stage 3	0.135	0.131	−3 %
k_f (psi/gpm$^{1.5}$), stage 1	0.640	0.631	−1 %
k_f (psi/gpm$^{1.5}$), stage 2	0.659	0.643	−2 %
k_f (psi/gpm$^{1.5}$), stage 3	0.788	0.738	−6 %

Stage 1 has the highest specific pressure drop in state 1 or 11. Additionally, stage 3 has the lowest specific pressure drop in state 1 or 11. Both imply that block A has the least friction. When multiple blocks with different properties are connected in parallel, the system will find the balance itself. For example, if blocks A-C are in stage 1, more feedwater would go to block A (because it is the most fluidic and permeable) than block B or C so that all the blocks connected in parallel share the same pressure differential. As a result, almost two distinct levels for stage 1 can be seen in Fig. 10(f); k_f is at a lower level when block A is included in stage 1 and a higher level when it is rotated out.

Stage 2 (blocks EF) consistently experiences a slightly larger friction loss in states 1–4 than in states 11–14, possibly due to different lengths of connection pipes.

The project team investigated the difference in block performance, including collecting conductivity profiles, completing physical inspections of vessels, membranes, brine seals and o-rings, and completing inspections of manifolds. No evidence of manufacturing defects or operational variations were identified.

3.3. Concentrate overshoot during transition

Fig. 7 shows a significant overshoot in brine concentration following a feed flow reversal in stage 2 and block rotation between stages 1 and 3 (e.g. state transition 3→14). However, no significant overshoot in brine concentration is observed if there is no feed flow reversal in stage 2 during state transition (e.g. 14→11). A qualitative explanation is provided below.

When FRRO reaches steady state at its full production, the salt concentration is monotonously increasing along the process (shown in Fig. 9). However, this is not the case when interstage booster pumps P3 and P4 are turned off temporarily and blocks are re-positioned. After P3 and P4 are turned back on and the system is maneuvered to its steady state, the spatial concentration profile in some blocks may have to be flipped, leading to a concentration wave propagating through the system and an overshoot at the outlet [28]. The magnitude of the overshoot is largely dependent on the difference between the initial and final concentration profiles in the system.

An inspection of two different state transition cases is shown in Fig. 11: (a) 14→11, (b) 3→14. When pumps P3 and P4 are turned off temporarily, the system in case (a) is on two stages. The first stage (i.e. blocks BC) has a recovery about the same value in full production (i.e. 45 %). The second stage (i.e. blocks EF), however, has a recovery in the range of 30–40 %, which is significant lower than its value in full production (i.e. 55 %) because the inter-stage pump P3 is off. If the whole system (i.e. blocks A-F) is simply treated as a black box, the average salt load before P3 and P4 are turned back on is lower than its steady state value at 90 % system recovery. When pumps P3 and P4 are turned off temporarily in case (b), it has only one stage (i.e. blocks AB), which has a recovery of 50–60 %, higher than its value in full production (i.e. 45 %). In this sense, the average salt load in all the blocks before P3 and P4 are turned back on is higher than its value at full production. The extra amount of salt has to flow out of the system before steady state is reached.

Concentration overshoot is further observed when the system goes back to full production. In case (a), when block D joins stage 1, its rear-end element becomes the lead element, whose concentration is 10 times of the feed at 90 % recovery. The coupled fluid flow and mass transfer results in a concentration wave propagating through all the six elements [28]. A concentration overshoot is expected at the outlet of block D. However, no conductivity meter is available at this particular location in the pilot test. The peak is instantaneously lowered because of the mixing of retentate streams from blocks B, C and D before the blended feed enters stage 2. The peak of the wave is further suppressed when it passes through stages 2 and 3 because they both have lower than normal salt load. In case (b), a similar concentration wave in block D will propagate through all the stages. The difference is that the mixing of retentate

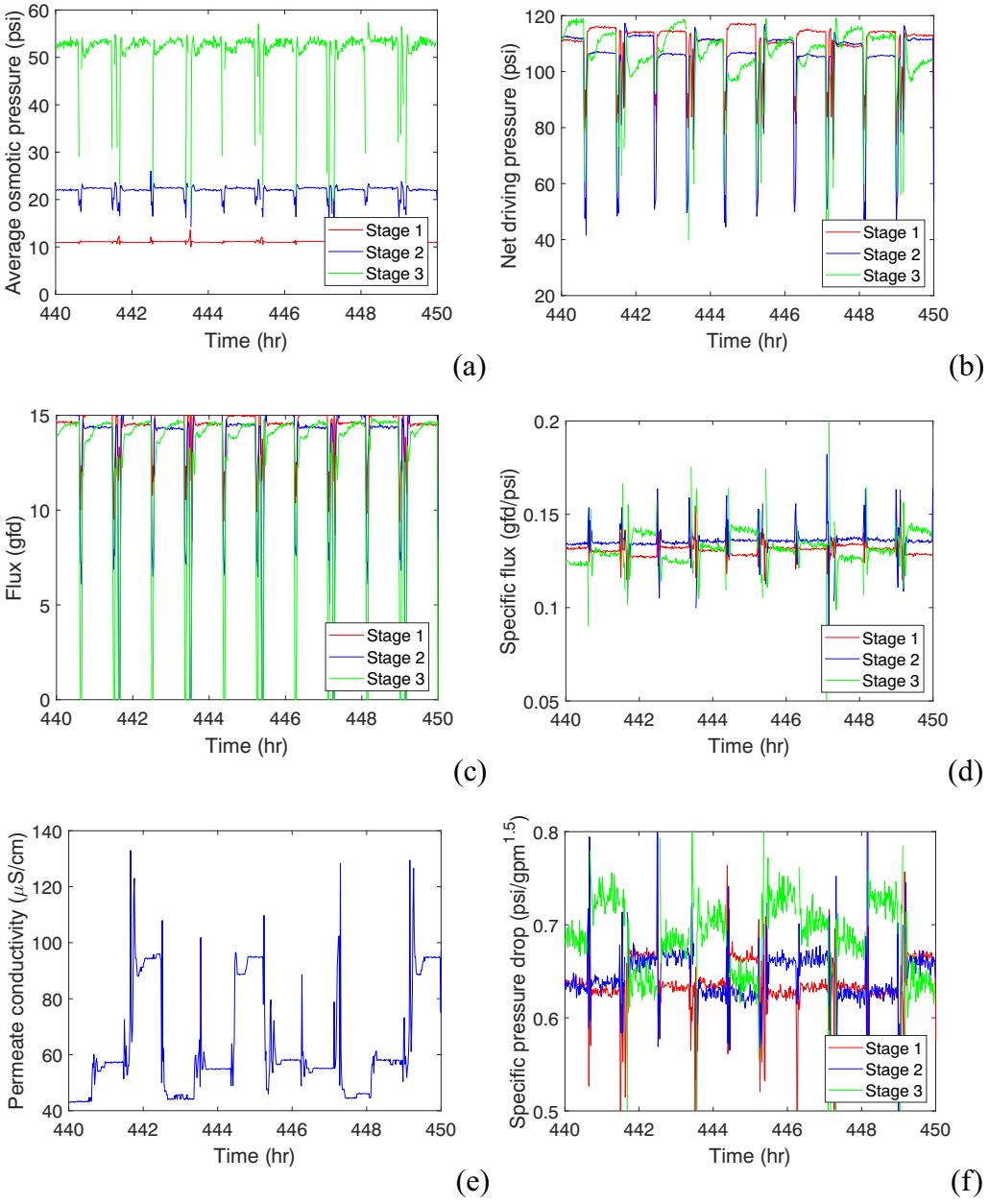

Fig. 10. (a) Average osmotic pressure, (b) NDP, (c) average flux, (d) specific flux, (e) permeate conductivity, and (f) specific pressure drop in each stage during 10 h of operation.

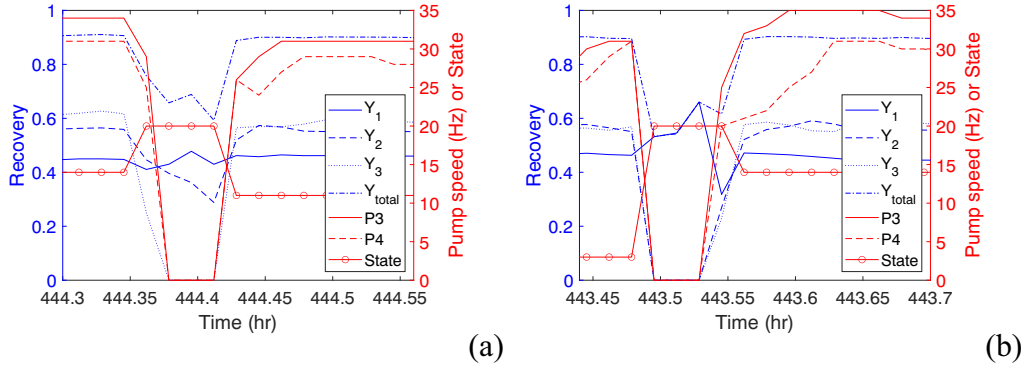

Fig. 11. Comparison of two types of state transitions. (a) 14→11. (b) 3→14.

streams from blocks A, B, and D does not lower the peak to the same extent because other blocks in stage 1 have a concentration higher than the one in case (a). Moreover, stage 2 has a flipped spatial concentration profile, which may intensify the peak. Even though stage 3 may attenuate the magnitude of the wave, overshoot at its outlet is inevitable. A comparison of initial and final concentration profiles in both transition cases is shown in Fig. 12.

A transient model shows that it takes a few space times for feed flow reversal to reach steady state [26]. A rough estimation of the space time is provided below. For one 73 sqft Toray TML10D RO element with 34 mil spacers, its liquid holdup volume is estimated to be 0.7 gal ($0.7 = 73 \times 0.034/2/12 \times 0.9 \times 7.48$, where 0.9 is the estimated void fraction of the feed channel). The feed flow per vessel (in parallel) is about 10, 8.25 and 7.5 gpm in each stage during full production. Using the liquid hold up per block of 4.2 gal ($4.2 = 0.7 \times 6$), the space time is calculated to be 0.42, 0.51, and 0.56 min for stage 1, 2, and 3. Pilot data show that the concentration overshoot generally occurs 4–5 min after the pumps P3 and P4 are turned back on.

Because of the concentration overshoot in FRRO, its peak brine concentration is 20 % greater than what would be expected in a conventional steady-state design at the same recovery. The concentration overshoot may adversely affect membrane performance despite that the rear-end elements are periodically flushed by the under-saturated fresh feed. It was found that the feed flow direction in stage 2 was reversed every 112 min in the pilot test. Future studies may consider to reduce the frequency or even eliminate periodic feed flow reversal in stage 2. Another possible way to suppress concentration overshoot is to temporarily reduce recovery before state transition.

3.4. Membrane performance degradation over a long-time period

The long-term performance of the FRRO pilot system is shown in Fig. 13. During this period, temperature is fairly constant (between 22 and 23 °C). To reduce noise in data processing, data associated with state 20 are not included. Initially, all the stages have more or less the same membrane permeability, because it was several days after a CIP event. However, as system fouls, both stages 1 and 3 observe a progressive decline in the specific flux. Moreover, they sort of mimic each other since they periodically share the same water quality. There is also a decline in the specific flux in stage 2, however, it is less severe because it treats less aggressive water than the other two stages.

Additionally, an increase in the specific pressure drop is clearly seen in stage 1. There appear to be two distinct curves of k_f because of different flow characteristics with and without block A discussed earlier. They both increase about 10 % after 18 days of operation at 90 %. There are also two distinct curves of k_f in the second stage, each corresponding to a different feed flow direction, and both slightly go up over time. Membrane autopsies indicated inorganic scaling, primarily calcium carbonate and silicate species and to a lesser extent the presence of calcium sulfate. Additionally, particulate fouling from colloidal iron and manganese that passed through insufficient pretreatment also contributed to performance reduction.

To maintain the system recovery, the feed pressures have to be elevated (about 12–15 % over 18 days of operation at 90 %) to compensate for ever-decreasing membrane permeability and ever-increasing friction loss. These appear to be consistent with conclusions in literature [29–31]. The hydraulic specific energy consumption (SEC), or $\left[Q_{f1}P_{f1} + Q_{f2}\left(P_{f2} - P_{f1} + P_{d1}\right) + Q_{f3}\left(P_{f3} - P_{f2} + P_{d2}\right)\right]/\left(Q_{f1} - Q_{b3}\right)$, is calculated to be 0.33–0.39 kWh/m^3. The actual SEC assuming a constant pump efficiency of 80 % is 0.41–0.49 kWh/m^3, which is at a low level. This confirms our previous study that energy consumption is less a concern than membrane fouling at 90 % recovery for low-salinity brackish water RO [28]. Interestingly, the permeate conductivity reduces over time, and the salt rejection becomes greater. Even though block A is relatively more permeable to salt than blocks BCD initially, the difference becomes smaller over time. It is speculated that fine particulate foulants may partially block the membrane surface and pores, resulting in reduced water and salt transport. One relevant example in literature is that RO membrane fouling caused an increase in *N*-nitrosodimethylamine (NDMA) rejection, which was explained by a densely packed fouling layer, whose clearance was too small for NDMA to go through [32].

3.5. Oscillation of specific flux

Even though the specific flux in each stage is noisy (due to variation in block performance) in Fig. 13(a), a periodic oscillation can be clearly seen. The time period is found to be 24 h, which obviously differs from the cycle time. The specific flux in stage 2 and temperature are presented in Fig. 14(a), indicating a strong correlation between them. The increased membrane permeability at a higher temperature is mainly due to the higher diffusion rate of water through the membrane [25]. Using a temperature correction factor (TCF) $= exp[2640(1/(T/[C] + 273.15) - 1/\ 298.15)]$, the specific flux is normalized to standard conditions of 25 °C and is shown in Fig. 14(b). The magnitude of oscillation is much smaller, but not eliminated, especially after occurrence of fouling.

It is found that an increase in temperature would lead to a higher passage of salts during 730–850 h. This is primarily due to an increase in the salt diffusion coefficient with temperature [25]. However, in this pilot test, the variation in block performance overshadowed the temperature effect most of the time.

The ROTEC's FRRO pilot test had a total online time of 144 days, approximately 106 days at 89 % or greater recovery and 15 consecutive days at 91 % recovery. There were five CIPs in the entire test period

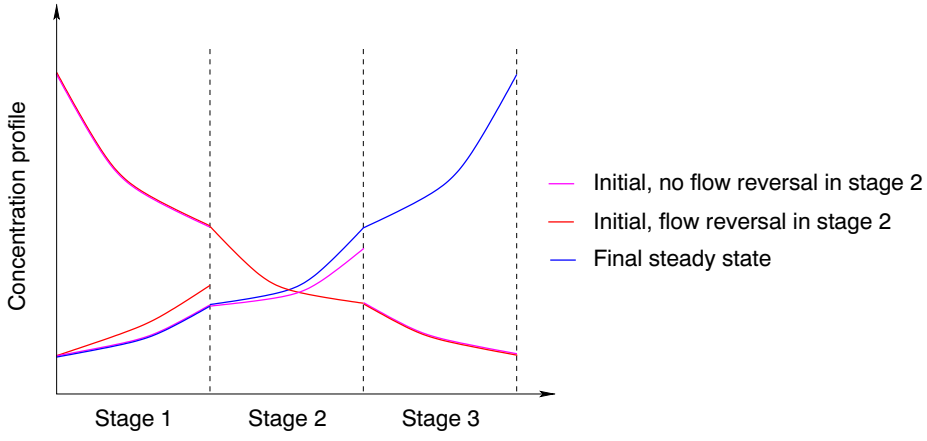

Fig. 12. Comparison of spatial concentration profiles before and after state transitions.

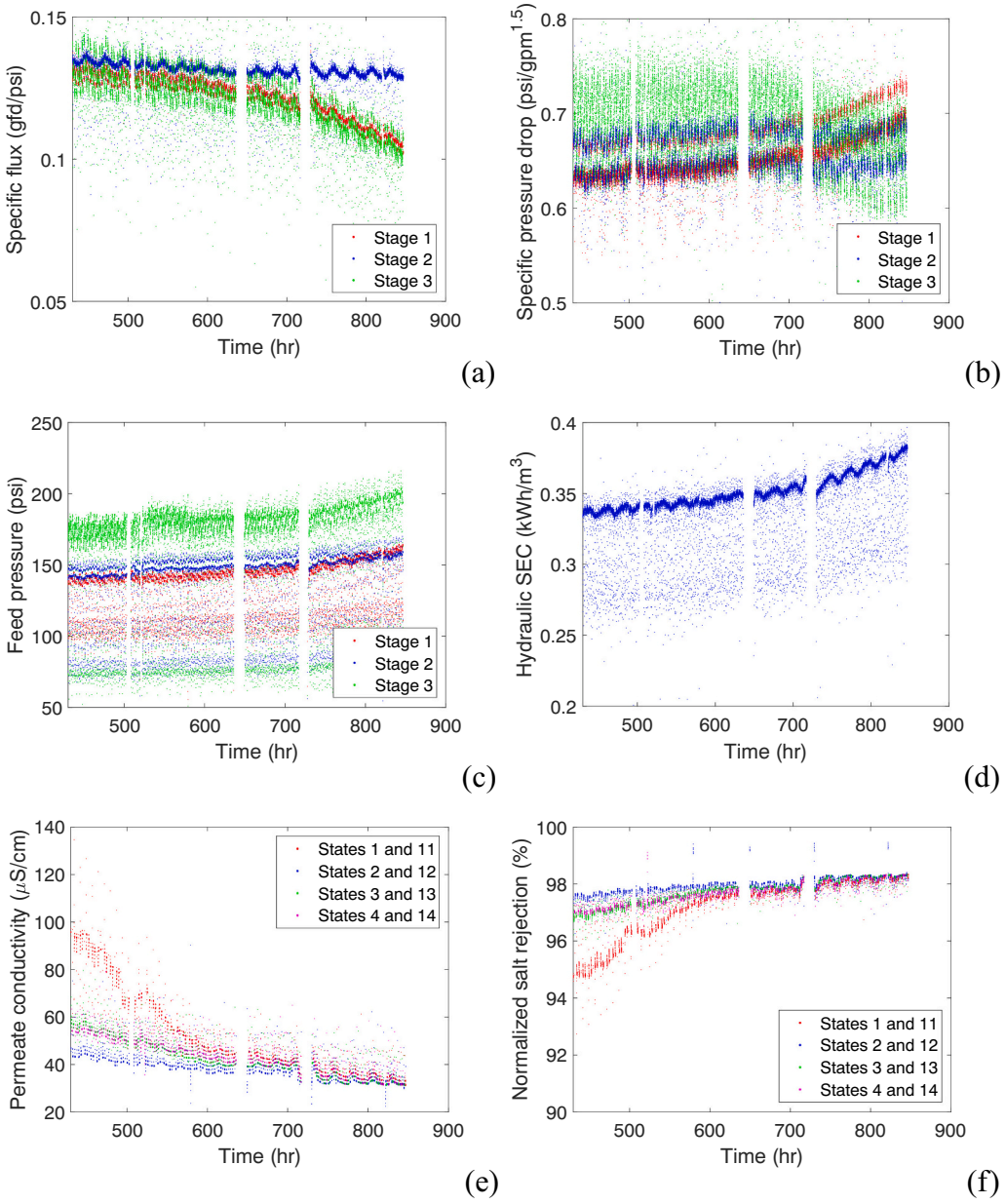

Fig. 13. Decline in specific flux, (b) increase in friction loss, (c) increase in feed pressure, (d) increase in hydraulic SEC, (e) decrease in permeate conductivity, and (f) increase in normalized salt rejection over a long period of operation.

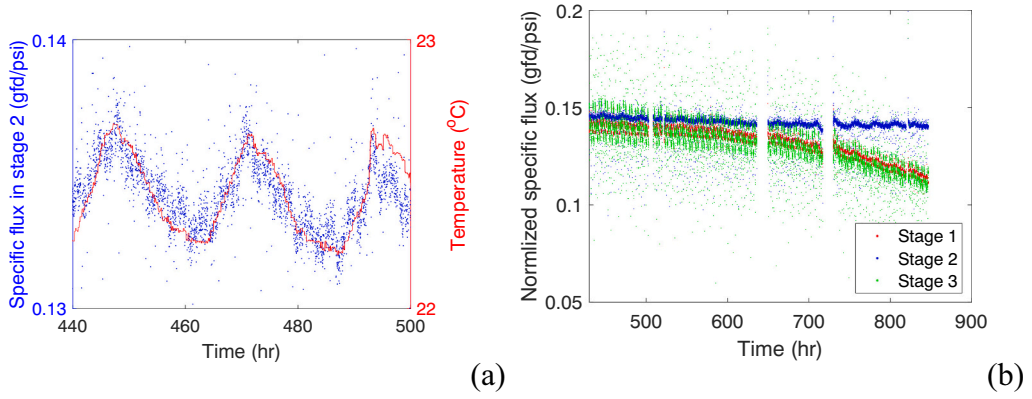

Fig. 14. (a) Correlation between specific flux in stage 2 and temperature. (b) specific flux normalized to the standard conditions of 25 °C.

triggered based on one or more of the following conditions being met: 1) decline of normalized specific flux of 15 %; 2) increase of normalized salt passage of 15 %; and 3) increase of normalized differential pressure of 15 % (See supplementary material for details). Typical pilot operation between CIP events was over 30 days, and the longest operation period was 42 days. Pilot performance appeared more stable while using the Vitec-4000. However, the operations team conducted more trouble-shooting during the first three months of operations due to water quality upsets in the pretreatment system, preventative maintenance on the pneumatic valves (i.e., burst air lines and unlocked throttling valves causing valves to open and close outside of the 8–10 s preferred operating window), and other mechanical issues. It is unclear if the anti-scalant dose was the primary differentiator for improved performance.

3.6. Full-scale plant retrofit

Following the completion of successful pilot testing in 2020, the City proceeded with the design and commissioning of full-scale retrofits of the existing RO system [33]. To mitigate colloidal iron and manganese fouling identified in the pilot testing, all of the original greensand media has been replaced with new media, and total iron and manganese is being maintained at a limit of 0.05 mg/L entering the RO system. The retrofitted skid will consist of three stages in a 43:21:9 configuration, each vessel housing six RO elements. Using the Toray TMG20D-440 membrane, the maximum feed flow will be 1900 gpm and flux of 12.8 gfd. A primary high-pressure RO feed pump will feed water into the first stage vessels, and interstage booster pumps between both second and third stages will boost pressures within the proceeding stages as well as modulate flow during the flow-transition sequences. Due to hydraulic limitations of the retrofitted skid, ten of the first stage vessels will remain in static mode. The first and third stage vessels plumbed for flow-reversal rotation are arranged in blocks of three vessels each assigned a letter A through N.

Just like the pilot system, the majority of the time the full-scale system will function in plug-flow mode whereby three blocks will be assigned into third stage by isolating specific pneumatic valves allowing the third stage feed flow to enter vessels in the opposite direction as the first stage blocks. Approximately every hour for 2 min, the system will enter a transition step whereby the third stage booster pump stops, the existing third stage blocks are isolated from third stage and reintroduced into the first stage system, and three new blocks are positioned to receive the third stage feed flow as the third stage booster starts operations again. Approximately 4 h will elapse before the original third stage blocks will return to the third stage. Every other transition step, the second stage pressure vessels' feed flow will reverse direction. If at any time the flow reversal process wants to be stopped and operations returned to conventional mode (e.g., 82–83 % recovery), operators can elect to shutdown the system, flush the elements with RO permeate, and return the system to operations in conventional mode only where the periodic flow reversal transition step does not occur. This flexibility provides the City risk mitigation and operational flexibility in the event the flow reversal process is not available. Different from the pilot system, the full-scale system has a reduced flow-transition time of 2 min at a recovery rate of 90 % during plug-flow operations. As a result, the actual recovery is 89.4 %, only slightly lower than the targeted value. Further optimization investigations are planned for the full-scale system to evaluate increasing the time between flow-reversal transitions in order to increase the actual recovery.

The total capital cost for retrofitting four existing conventional RO skids to flow-reversal is approximately $10 million, and the total annual operating cost in addition to existing operating costs is approximately $500,000. The total annual water production cost for the additional water produced at 90 % recovery is $1070 per acre-foot per year. The payback period of plant retrofit is estimated to be two years. We hope to report operating experience of the full-scale system in the future.

4. Conclusions

The block rotation and feed flow reversal in ROTEC's technology balance salt and foulant load across all stages and mitigate scaling formation, enabling a 90 % recovery with a reasonable CIP interval at City of Santa Monica's Arcadia WTP. As membrane fouls, there is a decline in the specific flux and an increase in the specific pressure drop. These lead to an increase in operating pressures over time. Nevertheless, the last stage pressure is usually 200 psi or lower at a 90 % recovery. After completing side-by-side testing of CCRO and FRRO pilots, the City moved forward with design and commissioning of full-scale retrofits of the existing RO system using ROTEC's FRRO technology. The CCRO experienced capricious scaling issues and required more constant oversight when recovery was pushed over 85 %.

A 20 % concentration overshoot is observed at the pilot scale every time the feed flow to stage 2 changes direction. It is recommended to investigate the effect of feed flow reversal frequency on membrane performance in full plant operation.

CRediT authorship contribution statement

Mingheng Li: Writing – review & editing, Writing – original draft, Software, Methodology, Formal analysis. **Alex Waite:** Writing – review & editing, Writing – original draft, Resources, Methodology, Investigation, Data curation. **Sunny Wang:** Writing – review & editing, Writing – original draft, Resources, Methodology, Investigation, Data curation.

Declaration of competing interest

The authors declare that they have no known competing financial interests or personal relationships that could have appeared to influence the work reported in this paper.

Data availability

Data will be made available on request.

Acknowledgements

Sunny Wang and Alex Waite would like to thank the manufacturer, contractor, and consultant team who spent many late nights and early mornings making the pilot project successful. Special thanks go to Omer Michaeli with ROTEC Ltd., Shaun Jameson with Walsh Construction, Adam Zacheis with Brown and Caldwell, Geohvanny Herrera and Gary Richinick with the City of Santa Monica, and all of their team members for their support.

Mingheng Li would like to acknowledge financial support from the National Science Foundation (CBET-2140946). Any opinions, findings, and conclusions or recommendations expressed in this material are those of the author and do not necessarily reflect the views of the National Science Foundation.

Appendix A. Supplementary data

Supplementary data to this article can be found online at https://doi.org/10.1016/j.desal.2024.117348.

References

[1] M. Qasim, M. Badrelzaman, N.N. Darwish, N.A. Darwish, N. Hilal, Reverse osmosis desalination: a state-of-the-art review, Desalination 459 (2019) 59–104.
[2] M. Busch, W.E. Mickols, Reducing energy consumption in seawater desalination, Desalination 165 (2004) 299–312.
[3] M. Elimelech, W.A. Phillip, The future of seawater desalination: energy, technology, and the environment, Science 333 (2011) 712–717.
[4] M. Li, B. Noh, Validation of model-based optimization of brackish water reverse osmosis (BWRO) plant operation, Desalination 304 (2012) 20–24.

[5] H. Gu, M.H. Plumlee, M. Boyd, M. Hwang, J.C. Lozier, Operational optimization of closed-circuit reverse osmosis (CCRO) pilot to recover concentrate at an advanced water purification facility for potable reuse, Desalination 518 (2021) 115300.
[6] P. Sanciolo, N. Milne, K. Taylor, M. Mullet, S. Gray, Silica scale mitigation for high recovery reverse osmosis of groundwater for a mining process, Desalination 340 (2014) 49–58.
[7] A. Antony, J.H. Low, S. Gray, A.E. Childress, P. Le-Clech, G. Leslie, Scale formation and control in high pressure membrane water treatment systems: a review, J. Membr. Sci. 383 (2011) 1–16.
[8] Z. Amjad, Scale inhibition in desalination applications: an overview, in: The NACE International Annual Conference and Exposition, 1996 (pp. NACE–96–230).
[9] A. Matin, F. Rahman, H.Z. Shafi, S.M. Zubair, Scaling of reverse osmosis membranes used in water desalination: phenomena, impact, and control; future directions, Desalination 455 (2019) 135–157.
[10] J. Rolf, T. Cao, X. Huang, C. Boo, Q. Li, M. Elimelech, Inorganic scaling in membrane desalination: models, mechanisms, and characterization methods, Environ. Sci. Technol. 56 (2022) 7484–7511.
[11] M. Li, Analysis and Design of Membrane Processes: A Systems Approach, AIP Publishing, Melville, New York, 2020.
[12] V. Sonera, J. Septon, A. Efraty, CCD series no-21: illustration of high recovery (93.8%) of a silica containing (57 ppm) source by a powerful technology of volume reduction prospects, Desalin. Water Treat. 57 (2016) 20228–20236.
[13] G. Lauer, Conditioning process and device for producing pure water, US Patent 5,690,829 (Nov. 25 1997).
[14] N. Pomerantz, Y. Ladizhansky, E. Korin, M. Waisman, N. Daltrophe, J. Gilron, Prevention of scaling of reverse osmosis membranes by "zeroing" the elapsed nucleation time. Part I. calcium sulfate, Ind. Eng. Chem. Res. 45 (2006) 2008–2016.
[15] M. Uchymiak, A.R. Bartman, N. Daltrophe, M. Weissman, J. Gilron, P. D. Christofides, W.J. Kaiser, Y. Cohen, Brackish water reverse osmosis (BWRO) operation in feed flow reversal mode using an ex situ scale observation detector (exsod), J. Membr. Sci. 341 (1–2) (2009) 60–66.
[16] A.R. Bartman, C.W. McFall, P.D. Christofides, Y. Cohen, Model-predictive control of feed flow reversal in a reverse osmosis desalination process, J. Proc. Contr. 19 (2009) 433–442.
[17] H. Gu, A.R. Bartman, M. Uchymiak, P.D. Christofides, Y. Cohen, Self-adaptive feed flow reversal operation of reverse osmosis desalination, Desalination 308 (2013) 63–72.
[18] http://smgov.net/uploadedFiles/Departments/Public_Works/Water/SWMP.pdf, Online; Accessed December 24, 2023, 2018.
[19] https://www.awcproton.com, Online; Accessed September 12, 2023.
[20] J. Utter, N. Lovell, Personal Communication, 2023.
[21] M. Li, Optimal plant operation of brackish water reverse osmosis (BWRO) desalination, Desalination 293 (2012) 61–68.
[22] M. Li, T. Bui, S. Chao, Three-dimensional CFD analysis of hydrodynamics and concentration polarization in an industrial RO feed channel, Desalination 397 (2016) 194–204.
[23] M. Li, Optimization of multitrain brackish water reverse osmosis (BWRO) desalination, Ind. Eng. Chem. Res. 51 (2012) 3732–3739.
[24] M. Li, Predictive modeling of a commercial spiral wound seawater reverse osmosis module, Chem. Eng. Res. Des. 148 (2019) 440–450.
[25] Dupont, FilmTec Reverse Osmosis Membranes Technical Manual. https://www.dupont.com/content/dam/dupont/amer/us/en/water-solutions/public/documents/en/45-D01504-en.pdf, 2020 (Online; accessed April 25, 2020).
[26] M. Li, A spatiotemporal model for dynamic RO simulations, Desalination 516 (2021) 115229.
[27] C. Bartels, R. Franks, S. Rybar, M. Schierach, M. Wilf, The effect of feed ionic strength on salt passage through reverse osmosis membranes, Desalination 184 (2005) 185–195.
[28] M. Li, N. Chan, J. Li, Novel dynamic and cyclic designs for ultra-high recovery waste and brackish water RO desalination, Chem. Eng. Res. Des. 179 (2022) 473–483.
[29] N. Peña, S. Gallego, F. Del Vigo, S.P. Chesters, Evaluating impact of fouling on reverse osmosis membranes performance, Desalin. Water Treat. 51 (2013) 958–968.
[30] E.M. Hoek, T.M. Weigand, A. Edalat, Reverse osmosis membrane biofouling: causes, consequences and countermeasures, npj Clean Water 5 (2022) 45.
[31] M.A. Ahmed, S. Amin, A.A. Mohamed, Fouling in reverse osmosis membranes: monitoring, characterization, mitigation strategies and future directions, Heliyon 9 (2023) e14908.
[32] T. Fujioka, H. Aizawa, H. Kodamatani, Fouling substances causing variable rejection of a small and uncharged trace organic chemical by reverse osmosis membranes, Environ. Technol. Innov. 17 (2020) 100576.
[33] https://www.waterworld.com/drinking-water/treatment/article/14281379/reversing-the-ro-flow-in-california, Online; Accessed September 18, 2023 (2022).